Molecular Catalysis 518 (2022) 112071

Contents lists available at ScienceDirect

Molecular Catalysis

journal homepage: www.journals.elsevier.com/molecular-catalysis

The effect of ferromagnetism on the CO activation over FCC crystal phase transition metal catalysts: Insights from DFT calculations

Guorong Jia [a,b,d], Lixia Ling [c], Riguang Zhang [a,b], Baojun Wang [a,*]

[a] State Key Laboratory of Clean and Efficient Coal Utilization, Taiyuan University of Technology, Taiyuan, Shanxi 030024, PR China
[b] Key Laboratory of Coal Science and Technology of Ministry of Education and Shanxi Province, Taiyuan University of Technology, Yingze West Street, Taiyuan, Shanxi 030024, PR China
[c] College of Chemistry and Chemical Engineering, Taiyuan University of Technology, Taiyuan 030024, PR China
[d] Department of Basic Courses, Shanxi Agricultural University, Taigu 030801, PR China

ARTICLE INFO

Keywords:
CO activation
Density functional theory
Metal catalysts
Unpaired *d*-orbital electrons
Ferromagnetism

ABSTRACT

In order to understand the relationship between the ferromagnetism and catalytic performance, three pathways of CO activation over transition metal catalysts (Co, Ni, Cu, Rh, Pd, Ag, Ir, Pt, and Au) have been studied by using density functional theory (DFT) calculations. It is shown that Co and Ni metal catalysts have better catalytic performance for CO activation than others. The density of states (DOS) and spin density plots reveal that Co and Ni metal possess ferromagnetism. So it is concluded that the catalytic activity connects with the metal ferromagnetism. To further confirm this deduction, the magnetic moments and Bader charge have been calculated when small molecules (CO, CHO, and COH) adsorbed on the Co and Ni metal surface, and the results shows that the electron transfer between the small molecules and metal catalysts happens on the unpaired *d*-orbital electrons (n_d) of the metal, which changes the magnetic moments of Co and Ni metal. Meanwhile, electron transfer also changes the catalytic performance of Co and Ni metal catalysts. Compared with the CO, the electron transfer of CHO and COH is more, the magnetic moments of metal changes greatly, and the carbon-oxygen bonds of CHO and COH are easier to break. So the magnetic moments of metal catalysts can be used as an indicator to select different metal catalysts.

Introduction

With the world's energy demands constantly increasing, the importance of conversion from syngas (CO and H_2) to hydrocarbons has been progressively recongnized for more than a century [1–3]. This conversion can be achieved by the means of Fischer-Tropsch synthesis (FTS). So particular attention has been paid to CO activation since it is the first step in the FTS process [4–6]. And the central discussion is to understand the CO activation mechanism. In generally, CO activation includes three main activation mechanisms: (i) CO direct dissociation mechanism; (ii) H-assisted CO dissociation mechanism through CHO; (iii) H-assisted CO dissociation mechanism through COH [7–11].

According to molecular orbital (MO) theory, CO activation on the metal surface results from electron donation (from CO to the metal via the 5σ MO) and back-donation (from the metal to CO via the 2π* MO) [12,13]. When CO adsorbed on the metal surface, the metal-carbon bond is formed, and the carbon-oxygen bond of CO is weakened even broken ultimately. The different transition metals (TM) possess the respective ability of CO activation because of each electronic properties [14].

It has been evidenced that the activity and selectivity of metal catalysts highly rely on structural sensitivity. For example, HCP (hexagonal close-packed) Co has a better CO activation ability than FCC (face centered-cubic) Co [15], but Ni metal catalyst with face-centered cubic (FCC) phase is more active than that with hexagonal close-packed (HCP) phase for CO activation [16]. Hao et al. [17] proved that FCC Rh has a higher activity than HCP Rh. It shows that metal crystal phase has an impact on the catalytic performance of metal catalysts.

Another performance of structural sensitivity for transition metal catalysts is: different crystal surface possesses their respective catalytic properties. The step site, which is the most common defect for metal catalysts, is widely believed to show good activity in many catalytic reactions [18–20]. For example, it is suggested that the Rh(211) surface

* Corresponding author at: Key Laboratory of Coal Science and Technology of Ministry of Education and Shanxi Province, Taiyuan University of Technology, Yingze West Street, Taiyuan, Shanxi 030024, PR China.
E-mail address: wangbaojun@tyut.edu.cn (B. Wang).

https://doi.org/10.1016/j.mcat.2021.112071

Available online 28 December 2021

shows a higher activity than the Rh(111) surface for the syngas conversion reaction [21]. Liu et al. [22] found that NO reduction can be enhanced on the stepped Ir(211) surface. Xu and Mavrikakis [23] proved that: the stepped Au(211) surface possesses a better catalytic activity for the adsorption and dissociation of O_2 than that on Au(111). It is shown that the Cu(211) surface is more favorable for the CO and CO_2 hydrogenation reactions [24]. Metal (211) surface, which possesses 3 atomic row wide (111) terraces and 1 atomic row wide (100) steps, has better catalytic performance for CO activation [25], because it has low coordination numbers (CN) of metal atom and the 4-fold hole site [26]. Moreover, it holds the B_5 active unit, which is regarded as the active unit of catalytic synthesis [27–30]. It is well known that CO direct dissociation is associated with the adsorption configuration of the product C or O atom. The four-fold hollow site can strongly adsorb the C atom and decrease the activation energy of CO direct dissociation [7]. And the B_5 active unit possesses the four-fold hollow site, so this unique structures lower the barrier of CO activation.

The conversion from syngas to hydrocarbons over the groupⅧ metal catalysts have been studied experimentally and it suggests that the order of conversion rate is: Ru>Fe>Co>Rh>Ni>Ir>Pt>Pd [31]. However, experimentally there are many factors affecting catalytic performance [32–34], and it is determined by both the physical and chemical properties of the metal catalysts under reaction environment. Theoretically it is found that Fischer-Tropsch synthesis over transition metal catalysts has a connection with the electronic properties of the catalysts, the value of $\Delta(1\sigma-4\pi)$ (carbon–oxygen separation energy) plays an important role in CO activation [35–37].

In recent years, some studies suggests that the performance of metal catalysts is related to ferromagnetism [38]. The number of unpaired *d*-orbital electrons (n_d) of transition metals lead to the ferromagnetism (such as Fe, Co and Ni) [39]. Experimentally it is shown that the selectivity and activity of Fe- and Co-based metal catalysts change with the unpaired *d*-orbital electron number, and the optimized CO conversion for the Fe- and Co-based metal catalysts are obtained when the value of n_d is 2.23 and 1.66, and the catalytic performance of metal catalysts change with metal magnetism [40]. Moreover, the absorption energy of CO over transition metal catalysts is associated with the unpaired *d*-orbital electron [41,42]. And the absorption of small molecules on the transition metals significantly affects the magnetic properties of transition metals [43–45], it indicates that the electron transfer between the small molecules and metal catalysts happen on the unpaired *d*-orbital electrons (n_d) of the metal. However, up to now, the performance of different transition metal catalysts for CO activation have not been studied. Does the ferromagnetism have a connection with the catalytic performance in theory?

In this work, we selected transition metal catalysts (Co, Ni, Cu, Rh, Pd, Ag, Ir, Pt, and Au) as research object in order to eliminate the influence of metal crystal phase. All of them possess FCC (face centered-cubic) crystal phase. And based on higher catalytic activity of metal (211) surface, we investigated CO activation performance on the metal (211) surface. The activation energy (E_a) of three pathways of CO activation on the nine metal surfaces were studied. Then the density of states (DOS) and spin density plots were illustrated in order to characterize the ferromagnetism. The magnetic moments and Bader charge were calculated when small molecules (CO, CHO, and COH) adsorbed on the Co and Ni metal surface. In addition, the electronic properties of small molecules (CO, CHO, and COH) were discussed.

2. Computational methods and models

2.1. Computational methods

DFT calculations were performed by applying the Vienna *ab* Initio Simulation Package (VASP) [46,47], where the generalized gradient approximation (GGA) with the function of Perdew-Burke-Ernzerhof (PBE) formalism was selected to treat the exchange correlation energy of the electrons [48,49]. The electronic wave functions were employed based on the plane waves with a cutoff energy of 400 eV. SIGMA = 0.2 eV was selected for the Gaussian smearing parameter. The convergence criteria for atoms forces were converged to be less than 0.03 eV/Å and electronic convergence was performed to 1×10^{-5} eV. The k-point grid of $3 \times 3 \times 1$ was employed to sample the Brillouin zone [50]. To locate the transition state, Climbing-Image Nudged Elastic Band method (CI-NEB) was used to obtain the minimum energy path [51,52], which were inserted four optimized iteratively intermediate images, and frequency analysis was confirmed for only one imaginary frequency of transition state structure.

The adsorption energy (E_{ads}) of the adsorbed species involved in CO activation were calculated as (1):

$$E_{ads} = E_{slab} + E_{adsorbate} - E_{adsorbate/slab} \quad (1)$$

Where $E_{adsorbate/slab}$ corresponds to the total energy of the slab with adsorbed species; E_{slab} corresponds to the energy of clean surface slab, and $E_{adsorbate}$ corresponds to the energy of molecule in the gas phase.

The activation barrier (E_a) and reaction energy (ΔH) of the elementary reaction were defined as (2) and (3):

$$E_a = E_{TS} - E_{IS} \quad (2)$$

$$\Delta H = E_{FS} - E_{IS} \quad (3)$$

Where E_{IS}, E_{TS}, and E_{FS} refer to the total energy of the initial, transition, and final state structure.

The *d*-band center was obtained by the Eq. (4)

$$\varepsilon_d = \frac{\int_{-\infty}^{+\infty} E\rho_d(E)\mathrm{d}E}{\int_{-\infty}^{+\infty} \rho_d(E)\mathrm{d}E} \quad (4)$$

Where ρ_d corresponds to the density of states projected on the *d*-orbitals of the metal atoms.

2.2. Surface model

For the metal (211) surface, the $p(2 \times 3)$ super cells were used to model it, and the periodic repeating slabs was 6 atomic layers, the bottom 2 layers of which were fixed at the bulk positions. The neighboring slabs were separated by means of the vacuum thickness of 15 Å so that the interactions could be avoided. The B_5 active site possesses five types of adsorption sites (Top, Bridge, Hole, HCP, and FCC) on the Metal (211) surface. And the coordination numbers (CN) of metal atom on the B_5 active site is marked in Fig. 1.

3. Results and discussion

3.1. Adsorption of the small molecules

The absorption energy of the small molecules with the zero-point vibrational energy (ZPE) correction, the corresponding most stable adsorption structures, and the key geometrical parameters of C, H, O, CH, CO, OH, CHO and COH on the metal (211) surface are displayed in Part 2 of Supplementary Material. The results shows that the small species prefer to absorb on B_5 site of metal (211) surface, and it reveals that B_5 site is the active unit for the CO activation over the metal (211) surface.

3.2. CO activation

3.2.1. CO direct dissociation mechanism

As one pathway for CO activation, CO direct dissociation mechanism on the transition metal catalysts or alloys catalysts has been studied extensively in the past years [53–56]. In this section, CO direct dissociation on different Metal (211) surface is considered. The activation

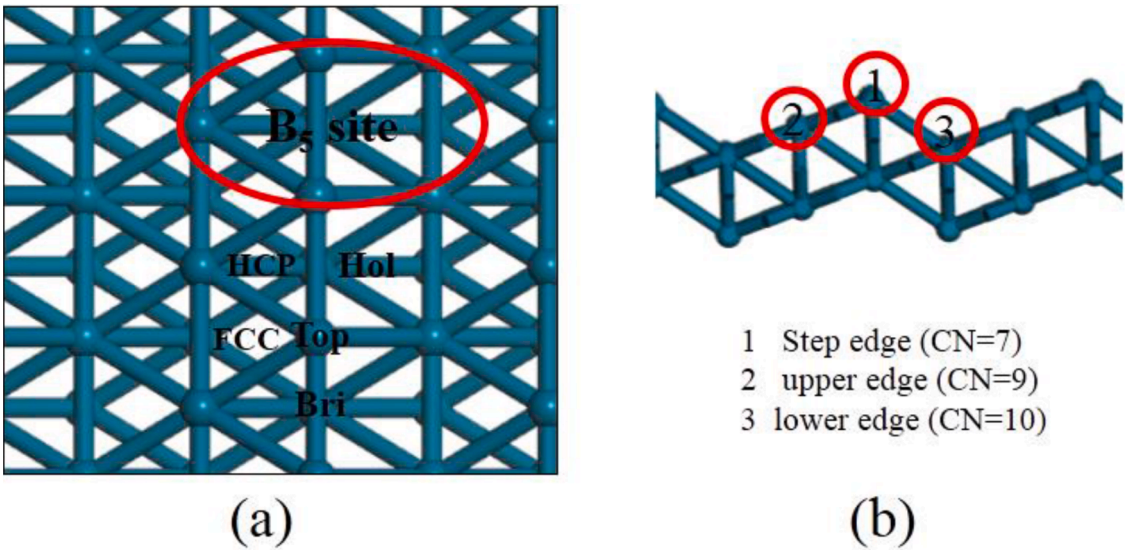

Fig. 1. (a) Top views of metal (211) surface with the B_5 site and the typical adsorption sites. (b) Side view of metal (211) surface and the coordination numbers (CN) of metal atom is marked.

barriers E_a, the reaction energy ΔH, the C=O distance of the transition state structure $d_{c\text{-}o}$, and the only imagination frequency of the transition state structure ω are shown in Table 1. And the potential energy diagram of CO direct dissociation are presented in Fig. 2. Correspondingly, the initial, transition, and final state structure of CO direct dissociation on different metal (211) surface are presented in Part 3 of Supplementary Material.

The huge variation of activation barrier E_a of CO direct dissociation indicates that CO direct dissociation depends on electronic properties of the metal catalysts. For the CO direct dissociation pathway, ordering these nine metals catalyst according to the activation barrier E_a, it presents the following sequence: Ni<Co<Rh<Cu<Ir<Pd<Ag<Pt<Au. Ni metal catalyst has the lowest activation barrier E_a of 2.02 eV. Secondly, Co metal catalyst has the activation barrier E_a of 2.28 eV. It suggests that the Co and Ni metal catalysts possess better CO activation ability. At the same time, the Co and Ni metal catalysts have the reaction energy ΔH of -0.33 and -0.04 eV. For the remaining FCC crystal phase transition metal catalysts, the activation barrier E_a are 0.99 eV higher at least than that of Co and Ni metal catalysts. Similarly, the reaction energy ΔH of the remaining metals are higher than that of the Co and Ni metal catalysts. It clearly suggests that CO direct dissociation is more favorable over the Co and Ni metal catalysts both kinetically and thermodynamically. The similar trend with the Brønsted-Evans-Polanyi (BEP) relation is obtained for the nine metal catalysts [57,58]: the greater the reaction energy ΔH, the higher the activation barrier E_a. It is widely known that the activation barrier E_a is associated with the adsorption configuration of the product C or O atom. For C atom, the most stable adsorption site is the four-fold hollow; but for O atom, there is little difference in absorption energy at different site (especially the Bri, HCP and FCC site). And the absorption energy of O atom is much lower than that of C atom (as showed in Part 2 of Supplementary Material), so the O atom easily migrates among different sites at the transition state. Furthermore, there are wide variations in the absorption energy of C and O atom for the nine metal catalysts. And it results in the great difference of C-O distance at the transition state structure for the nine metal catalysts. For the Rh, Cu, Ir, and Pd metal catalysts, they have the modest E_a of CO direct dissociation. It is noteworthy that: for the Ag, Pt, and Au metal catalysts, the activation barriers of CO direct dissociation are so high that CO is difficult to dissociate via this pathway.

Table 1
The activation barriers (E_a, eV) and reaction energy (ΔH, eV) for the CO direct dissociation: CO=C+O, $d_{c\text{-}o}$ (in Å) is the C=O distance of the transition state structure,ω (in cm^{-1}) is the only imagination frequency of the transition state structure.

Surface	CO=C+O			
	E_a	ΔH	$d_{c\text{-}o}$	ω
Co(211)	2.28	−0.33	1.96	386
Ni(211)	2.02	−0.04	3.17	190
Cu(211)	3.63	1.78	2.16	139
Rh(211)	3.27	0.59	2.00	492
Pd(211)	4.91	1.07	1.95	515
Ag(211)	5.12	4.18	3.77	193
Ir(211)	3.95	1.33	2.04	445
Pt(211)	5.13	2.11	2.21	351
Au(211)	5.24	4.09	3.01	160

3.2.2. *H-assisted CO dissociation mechanism through CHO*

CO is hydrogenated to form CH and O via CHO is often regarded as a CO activation pathway [59,60]. In this section, the reaction of CO+H=CHO and CHO=CH+O are studied. The activation barriers E_{a1} and the reaction energy ΔH_1 for the reaction of CO+H=CHO, the activation barriers E_{a2} and the reaction energy ΔH_2 for the reaction of CHO=CH+O, and the total activation energy E_{total} for the CO+H=CH+O process are listed in Table 2. Correspondingly, the configurations of the co-adsorption of CO and H, the intermediate CHO, the co-adsorption of CH and O, the transition state, and the potential energy diagram of H-assisted CO dissociation mechanism through CHO over different metal catalysts are presented in Part 4 of Supplementary Material.

For the first elementary step of CO+H=CHO (as shown in Table 2), the activation barriers E_{a1} of Au, Ag, and Cu metal catalysts are 0.69, 0.79, and 1.06 eV, respectively. It reveals that the group IB elements are easy to form CHO via CO and H. For the Co and Ni metal catalysts, the activation barriers E_{a1} are 1.06 and 1.36 eV, both of them are modest for forming CHO via CO and H.

For the second elementary step of CHO dissociation to CH and O (as shown in Table 2), The Co and Ni metal catalysts have the activation barriers E_{a2} of 0.97 and 1.56 eV. It is found that Co and Ni metal catalysts can easily make CO activation via CHO and break the C=O bond. For the Ag and Au metal catalysts, the activation barriers are as high as 4.80 and 4.67 eV. It reveals that Ag and Au metal catalysts are difficult to break the C=O bond via CHO. It is worth noting that the C=O bond in CHO (CHO=CH+O) can be cleaved more easily than that in CO over all metal catalysts.

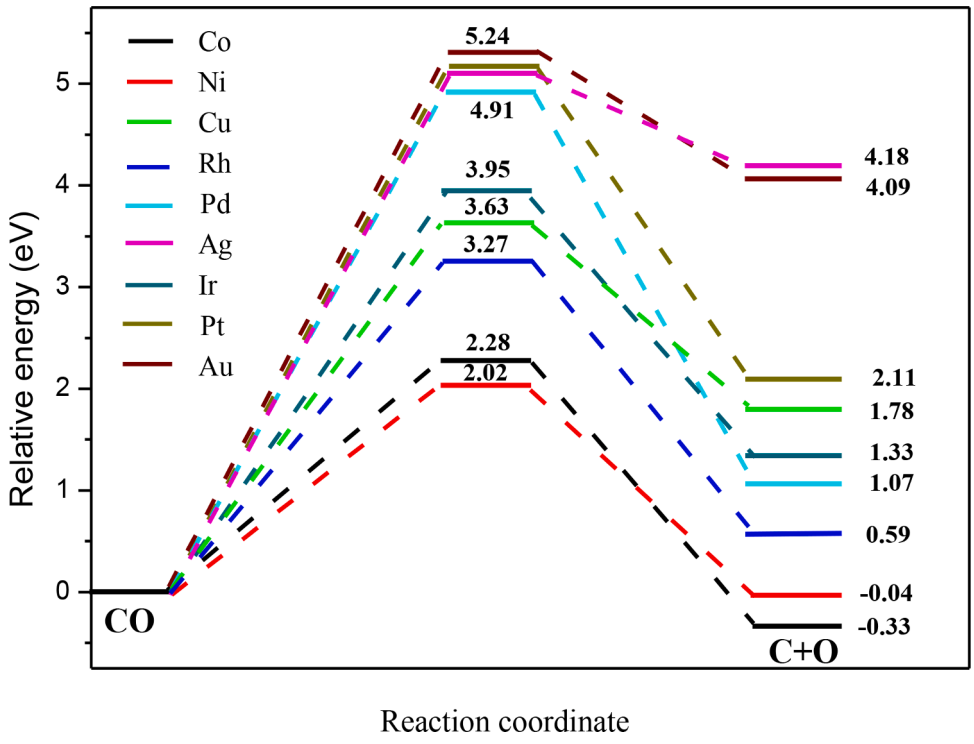

Fig. 2. The potential energy diagram of CO direct dissociation over metal (Co, Ni, Cu, Rh, Pd, Ag, Ir, Pt, and Au) catalysts.

Table 2
The activation barriers (E_{a1}, eV) and the reaction energy (ΔH_1, eV) for the reaction of CO+H=CHO, the activation barriers (E_{a2}, eV) and the reaction energy (ΔH_2, eV) for the reaction of CHO=CH+O, and the total activation energy (E_{total}, eV) for the CO+H=CH+O process.

Surface	CO+H=CHO		CHO=CH+O		CO+H=CH+O
	E_{a1}	ΔH_1	E_{a2}	ΔH_2	E_{total}
Co(211)	1.06	1.00	0.97	−1.22	1.97
Ni(211)	1.36	1.07	1.56	−0.73	2.63
Cu(211)	1.06	0.69	2.06	0.27	2.75
Rh(211)	1.40	0.91	3.14	−0.12	4.05
Pd(211)	1.78	1.18	2.60	0.75	3.78
Ag(211)	0.79	0.21	4.80	2.36	5.01
Ir(211)	1.71	0.78	2.03	0.36	2.81
Pt(211)	1.57	1.03	2.93	1.25	3.96
Au(211)	0.69	0.01	4.67	2.87	4.68

Table 3
The activation barriers (E_{a3}, eV) and the reaction energy (ΔH_3, eV) for the reaction of CO+H=COH, the activation barriers (E_{a4}, eV) and the reaction energy (ΔH_4, eV) for the reaction of COH=C+OH, and the total activation energy (E_{total}, eV) for the CO+H=C+OH process.

Surface	CO+H=COH		COH=C+OH		CO+H=C+OH
	E_{a3}	ΔH_3	E_{a4}	ΔH_4	E_{total}
Co(211)	2.05	0.91	0.84	−0.96	2.05
Ni(211)	2.11	0.99	1.04	−0.81	2.11
Cu(211)	2.36	1.24	1.69	0.09	2.93
Rh(211)	1.99	1.13	1.17	−0.61	2.30
Pd(211)	1.89	0.88	1.65	−0.05	2.53
Ag(211)	2.91	1.46	2.58	1.22	4.04
Ir(211)	1.88	0.90	1.59	−0.29	2.49
Pt(211)	1.81	0.72	1.90	0.47	2.62
Au(211)	2.18	0.76	2.62	1.66	3.38

Based on the above analysis about two elementary steps, according to the total activation energy E_{total} for the CO+H=CH+O process, the presented order is: Co<Ni<Cu<Ir<Pd<Pt<Rh<Au<Ag. The overall activation barrier varies from 1.97 to 5.01 eV for the nine catalysts. For the Co and Ni metal catalysts, the total activation energy E_{total} are 1.97 and 2.63 eV. Thus, it is assumed that the Co and Ni metal catalysts are favorable for CO activation via CHO to CH. In addition, however, it shows that this dissociation pathway is unfavorable for Ag and Au metal catalysts.

3.2.3. *H-assisted CO dissociation mechanism through COH*

CO is hydrogenated to produce C and OH via COH is also an important CO activation pathway [10,61]. In this section, the reaction of CO+H=COH and COH=C+OH are studied. The activation barriers E_{a3} and the reaction energy ΔH_3 for the reaction of CO+H=COH, the activation barriers E_{a4} and the reaction energy ΔH_4 for the reaction of COH=C+OH, and the total activation energy E_{total} for the CO+H=C+OH process are displayed in Table 3. Correspondingly, the optimized co-adsorbed structures of CO and H, the intermediate COH, and the co-adsorbed configurations of the C and OH, the transition state and the potential energy diagram of H-assisted CO dissociation mechanism through COH over different metal surface are presented in Part 5 of Supplementary Material.

For the reaction of CO+H=COH, the activation barrier E_{a3} ranges from 1.81 to 2.91 eV, which indicates that COH formation is weakly electron sensitive (as shown in Table 3). The activation barriers E_{a3} of Pt, Ir, and Pd metal catalysts are 1.81, 1.88, and 1.89 eV, respectively; For the Co and Ni metal catalysts, the activation barriers E_{a3} are 2.05 and 2.11 eV, which are modest for forming COH via CO and H; The activation barriers E_{a3} of Au, Cu, and Ag metal catalysts are 2.18, 2.36, and 2.91 eV, respectively, and they are higher than that of other transition metal catalysts.

For COH dissociation to C and OH, The Co and Ni metal catalysts have the activation barriers E_{a4} of 0.84 and 1.04 eV (as displayed in Table 3). It is suggested that Co and Ni metal catalysts favor the CO activation via COH. The activation barriers E_{a4} of Ag and Au metal catalysts are 2.58 and 2.62 eV, which are higher than that of other metal catalysts. It is worth noting that the activation barrier of COH for the broken of C=O bond (COH=C+OH) becomes lower on all metal catalysts than that of CO.

Based on the above calculation for H-assisted CO dissociation mechanism through COH, according to the total activation energy (E_{total}) for the CO+H=C+OH process, the displayed order is: Co<Ni<Rh<Ir<Pd<Pt<Cu<Au<Ag. Co and Ni metal catalysts are favorable for the CO activation via COH. The total activation energy (E_{total}) varies from 2.05 to 4.04 eV. For the Ag and Au metal catalysts, it is difficult to break the C=O bond via COH.

3.3. General discussions on CO activation

It is indicated that the transition metal situated in the right of the periodic table (such as Cu and Pd) show weak ability for CO direct dissociation, the C=O bond is un-cleaved during CO hydrogenation and methanol is its main product [36]. The transition metals situated in the left of the periodic table (such as Mo and W) show strong ability for CO direct dissociation, but they form metal carbides subsequently [62,63]. Fe, Co, and Ni metals are suitable for CO activation. CH_4 is the main product over Ni-based catalysts for it is disadvantageous to the C–C coupling [64], Fe and Co metals favor the production of long-chain hydrocarbons and are used for FT synthesis. It is interested that they all possess ferromagnetism. Theoretically the activation barriers E_a of CO direct dissociation is 1.09 eV for Fe(100) surface, it indicates that Fe metal catalyst has better CO activation ability [65], However, Fe metal only possesses one crystallographic structures: the body centered cubic (BCC) phase, and it does not been considered in order to eliminate the influence of structure sensitivity (metal crystal phase) in this paper.

In our study, the activation barriers (eV) of CO direct dissociation, the total activation energy (eV) of H-assisted dissociation mechanism through CHO and COH over different metal catalysts are displayed in Fig. 3. With regard to this three mechanisms, Co and Ni metals are more advantageous than other metal catalysts for CO activation. For Co metal catalyst, the optimal path for CO activation is H-assisted CO dissociation mechanism through CHO. For the Ni metal catalyst, CO direct dissociation is preferable for CO activation. For the group IB elements (especially the Ag and Au metal), the CO hydrogenation to CHO is easier, but it is difficult to break the C=O bond via this three pathway. The results is consistent with the past reports [36,66]. For the Rh, Pd, Ir, and Pt metal catalysts, H-assisted CO dissociation mechanism through COH is favorable for CO activation. After CO hydrogenated to CHO or COH, the activation energy (E_a) of broken the C=O bond become lower than that of CO for all metal catalysts.

3.4. Electronic properties analysis

For the CO activation, Co and Ni metal catalysts are more advantageous than other FCC crystal phase transition metal catalysts. Recently some research shows that the performance of metal catalysts is related to magnetism. It is noteworthy that Co and Ni metal catalysts possess ferromagnetism. The density of states (DOS) of the metal catalysts (Co, Ni, Cu, Rh, Pd, Ag, Ir, Pt, and Au) have been analyzed in Figs. 4 and S15. It is shown that the DOS of spin-up states and spin-down states are unsymmetric for the Co and Ni metal catalysts, so the Co and Ni metal perform metal ferromagnetism. However, for the Cu, Rh, Pd, Ag, Ir, Pt, and Au metal, the DOS of spin-up states and spin-down states are symmetric, and it perform non-ferromagnetism. Moreover, we have analyzed spin density plots of Co, Ni, and Cu metal catalysts (as shown in the Fig. 5). The copper metal is selected as a comparison. For the Co and Ni metal catalysts, the spin-up density is uniformly distributed on the each atom. But for the Cu metal catalyst, it includes the spin-up and the spin-down density, and the spin-up and the spin-down density is equal, so the Cu metal catalysts perform non-ferromagnetism.

Furthermore, The Bader charge from metal catalysts to small molecules ($\triangle q$, e) when small molecules absorbed on the metal surface is studied (as shown in Tables 4 and S11). It is showed that Co and Ni metal have more charge transfer than the other metal catalysts, which indicate that there is stronger interaction between small molecules and Co and Ni metal catalysts. Transition metals (Cu, Rh, Pd, Ag, Ir, Pt, and Au) possesses no magnetism, when small molecules (CO, CHO, and COH) absorbed on the metal surface, the magnetic moments of this metal catalysts is unchanged. The magnetic moments for Co and Ni metal catalysts (m_{total}, μB) are calculated (as presented in Table 4). The Co and Ni metal catalysts perform significantly ferromagnetism (m_{total}=62.24 μB for Co catalyst and m_{total}=24.09 μB for Ni catalyst). The model of metal (211) surface has 36 atoms, so the magnetic moments for each Co

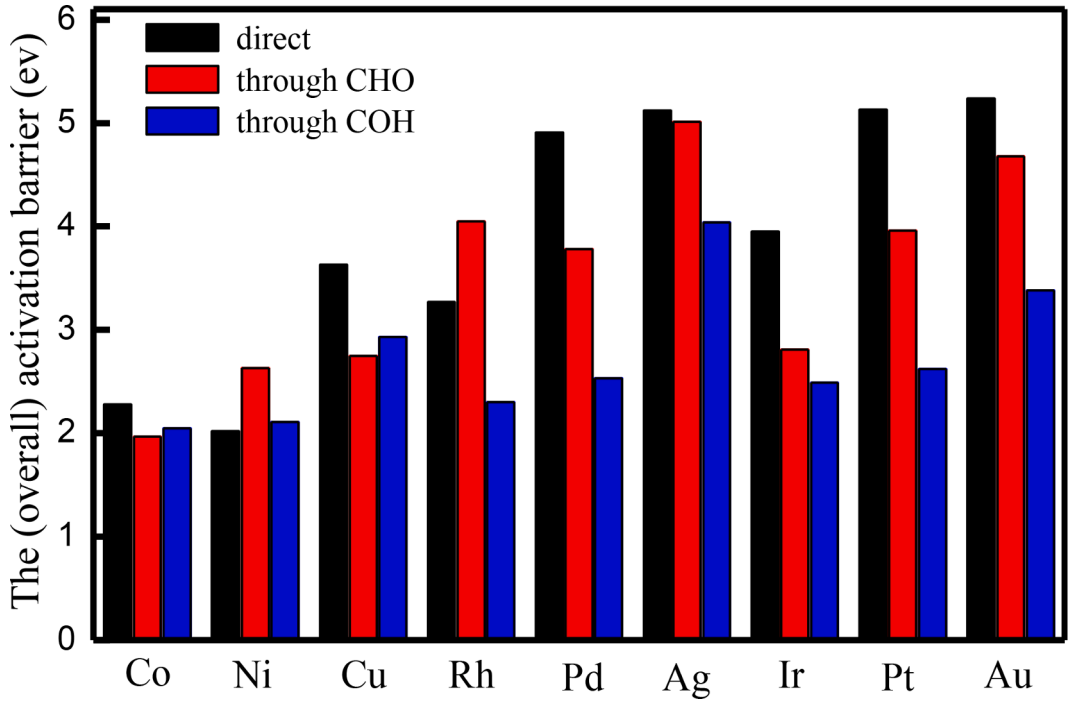

Fig. 3. The activation barriers (eV) of CO direct dissociation (black), the total activation energy (eV) of H-assisted dissociation mechanism through CHO (red) and COH (blue) over different metal catalysts.

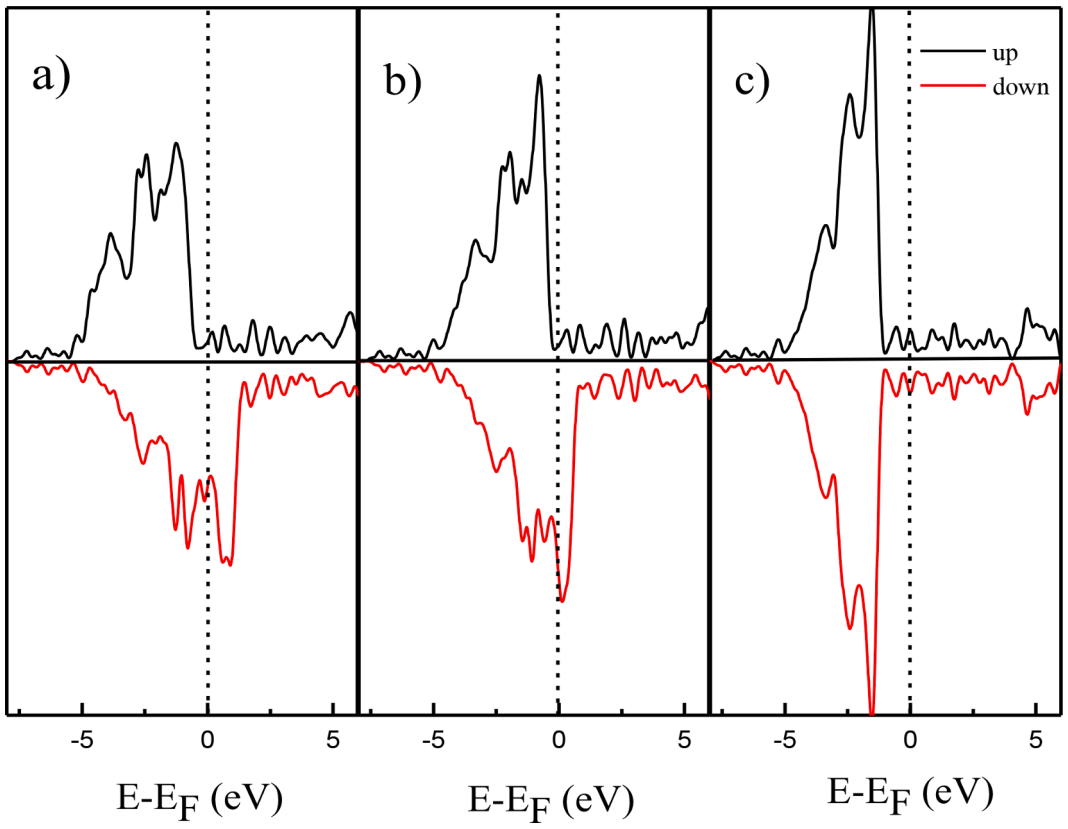

Fig. 4. (a) DOS for Co, (b) DOS for Ni, (c) DOS for Cu, The black line denote spin-up states and the red line denote spin-down states; the vertical dash lines indicate Fermi energy level.

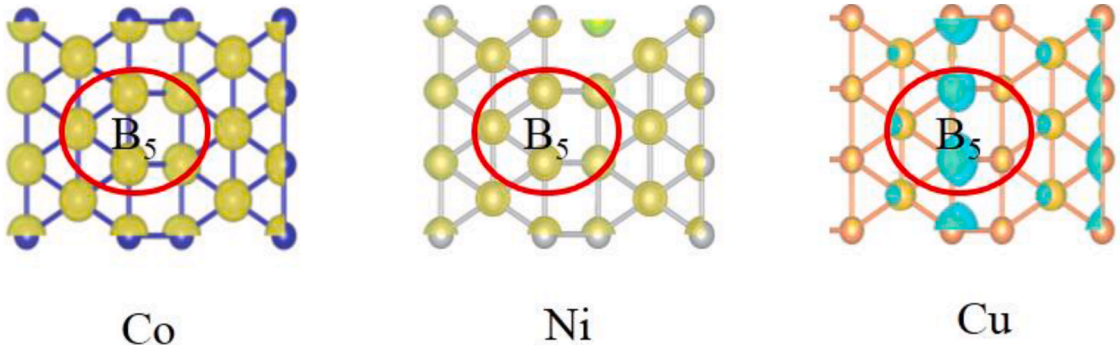

Fig. 5. Spin density plots for Co, Ni, and Cu metal catalysts; the spin-up density denoted by yellow and the spin-down density denoted by blue-green (the isosurface value of 0.03 e Å^{-3} was chosen).

Table 4
The magnetic moments for Co and Ni metal catalysts (m_{total}, μB) and each Co and Ni atom ($\overline{m}$, μB), the magnetic moments for metal catalysts (m'_{total}, μB) and the variation of the magnetic moments ($\triangle m$, μB) when CO absorbed on the metal surface ($\triangle m$, μB), and the Bader charge from metal catalysts to small molecules ($\triangle q$, *e*).

Metal	Co	Ni
m_{total}	62.24	24.09
$\overline{m}$	1.72	0.67
m'_{total}(CO)	61.66	23.58
$\triangle m$	−0.58	−0.51
$\triangle q$	−0.24 *e*	−0.20 *e*

and Ni atom ($\overline{m}$, μB) are 1.72 and 0.67 μB, which are in consistent with previous study [67,68]. After the CO absorbed on the metal surface, the magnetic moments of Co and Ni metal catalysts decline 0.58 and 0.51 μB, respectively. It probably results from the election transfer between the small molecules and metal catalysts. The Bader charge shows that Co metal catalyst donates 0.24 *e* to CO, and Ni metal catalyst donates 0.20 *e* to CO. The decrease of the ferromagnetism of Co and Ni catalysts results from the number of unpaired *d*-orbital electrons (n_d). So it is concluded that electron transfer between the metal catalysts and CO happens on the *d*-orbital of metal, and there is a subtle relationship between the metal ferromagnetism and catalytic activity for the CO activation.

Moreover, when the CHO absorbed on the metal surface, the magnetic moments of Co and Ni metal catalysts decline 0.69 and 0.85 μB, respectively (as presented in Table 5). The Bader charge shows that Co metal catalyst donates 0.34 *e* to CHO, and Ni metal catalyst donates 0.26 *e* to CHO. After the COH absorbed on the metal surface, the magnetic

Table 5
The magnetic Moments for metal catalysts (m'_{total} , μB) and the variation of the magnetic moments (△m, μB) when CHO or COH absorbed on the metal surface, and the Bader charge from metal catalysts to small molecules (△q, e).

Metal	Co	Ni
m'_{total}(CHO)	61.55	23.24
△m	−0.69	−0.85
△q	−0.34 e	−0.26 e
m'_{total}(COH)	60.94	22.45
△m	−1.30	−1.64
△q	−0.53 e	−0.44 e

moments of Co and Ni metal catalysts decline 1.30 and 1.64 μB, respectively. The Bader charge shows that Co metal catalyst donates 0.53 e to COH, and Ni metal catalyst donates 0.44 e to COH.

It is worthy noted that the magnetic moments of metal catalysts is related to the electron transfer between the metal and small molecules. The sequence of the electron transfer between metal and the absorbed small molecules is: $\triangle q_{(CO)}<\triangle q_{(CHO)}<\triangle q_{(COH)}$, and the order of the variation of the magnetic moments (△m) is: $\triangle m_{(CO)}<\triangle m_{(CHO)}<\triangle m_{(COH)}$. With the electron transfer between the metal and small molecules increasing, the variation of the magnetic moments enlarges. Meanwhile, there is a liner relationship between the catalytic activity and variation of the magnetic moments. After CO hydrogenated to CHO or COH, the order of the activation barrier (E_a) of broken the C=O bond is: $E_{a(COH)}<E_{a(CHO)}<E_{a(CO)}$. The electron transfer between CHO (or COH) and metal catalysts is more than that of CO, the carbon-oxygen bond of CHO and COH is easier to break on the metal catalysts. So it can be concluded that: the more electron transfer between the metal and small molecules, the greater change of metal ferromagnetism, and the catalytic activity increases. In other words, the greater change of ferromagnetism when small molecules absorbed on the metal surface, the higher catalytic activity of metal catalysts.

The properties of transition metals closely associate with the empty d-orbitals and d-electrons [69,70], so the d-band center (ε_d) for the Ni and Co metals when small molecules (CO, CHO, and COH) absorbed on their surface have been calculated and analyzed (as shown in Fig. 6). The d-band center (ε_d) for the Ni and Co metals are -1.19 and -1.26, which are consistent with the -1.17 and -1.29 reported by Ruban et al. [71]. When small molecules

(CO, CHO, and COH) absorbed on the Co metal, the d-band center (ε_d) are −1.26, −1.28, and −1.29, respectively. Similarly, when small molecules (CO, CHO, and COH) absorbed on the Ni metal, the d-band center (ε_d) are −1.30, −1.31, and −1.33, respectively. It is presented that the d-band center (ε_d) downshifts after small molecules absorbed on Co and Ni metal. It is interesting that there is a liner relationship between the d-band center (ε_d) and activation barrier (E_a) for Co and Ni metal catalysts. The sequence of the d-band center (ε_d) is: $\varepsilon_{d(COH)}<\varepsilon_{d(CHO)}<\varepsilon_{d(CO)}$, The order of activation barrier (E_a) is: $E_{a(COH)}<E_{a(CHO)}<E_{a(CO)}$. It is revealed that: the more the downshift of the d-band center (ε_d), the higher the catalytic activity of metal.

On the other hand, when CO hydrogenated to CHO or COH, the electronic properties of small molecule changes (as presented in Table 6). Compared with the CO, the level of HOMO (highest occupied molecular orbital) [72,73] of CHO and COH is shifted upward, and the

Table 6
The energy (in eV) of HOMO,LUMO,GAP of CO,CHO and COH.

	CO	CHO	COH
E_{LUMO}	−1.85	−3.18	−2.48
E_{HOMO}	−8.84	−4.81	−3.90
GAP	6.99	1.63	1.42

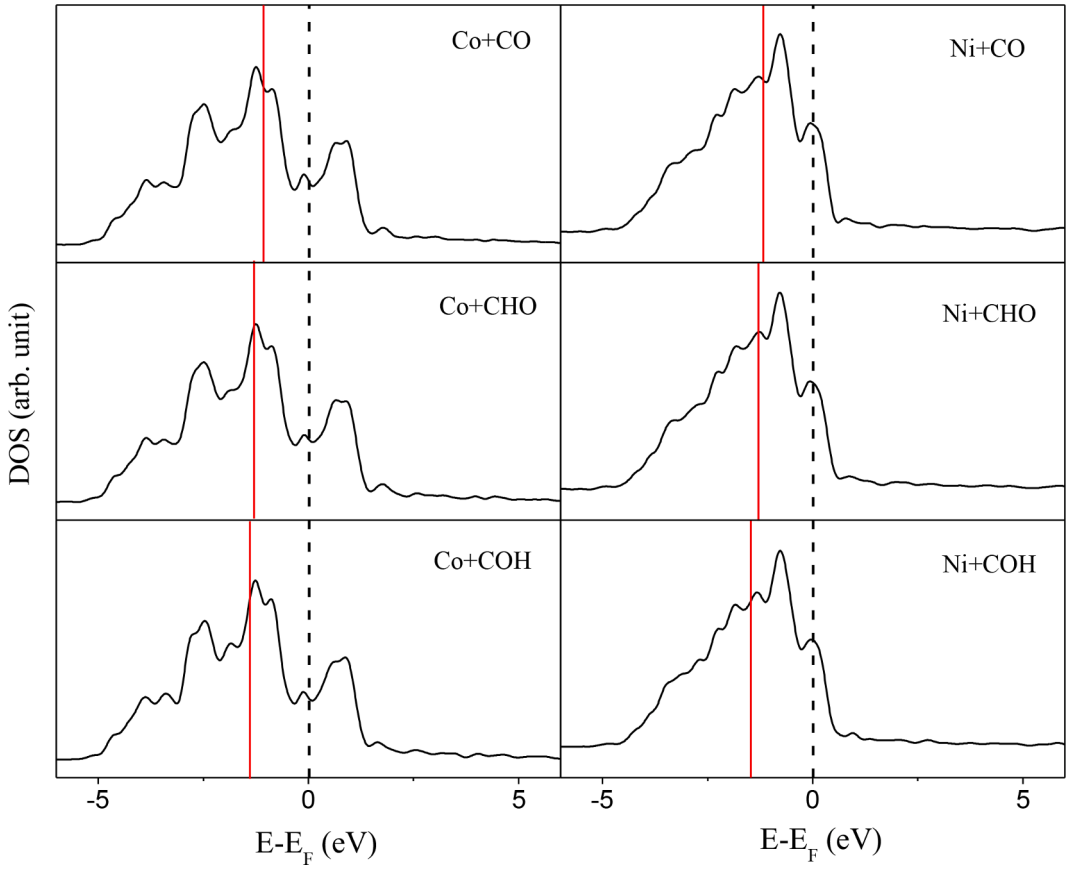

Fig. 6. The (ε_d) for the Ni and Co metals when small molecules (CO, CHO, and COH) absorbed on their surface, the black dotted line corresponds to the Fermi level.

level of LUMO (lowest unoccupied molecular orbital) of CHO and COH is shifted downward, so the GAP of HOMO and LUMO become smaller. The order of the energy of the GAP is: $GAP_{(COH)}<GAP_{(CHO)}<GAP_{(CO)}$, it indicates that CHO and COH are more active than CO. As a result, CHO and COH are easier to interact with the metal catalysts than CO, which intensifies the electron transfer between the metal and small molecules.

Through the above calculation results, it is shown that: when small molecules absorbed on the metal catalysts, electron transfer takes place on the *d*-orbital of metal catalyst. As a result, the ferromagnetism performed by transition metals changes. Meanwhile, the performance of metal catalysts also varies. So it is concluded that the metal ferromagnetism connects with catalytic activity for the metal catalysts.

4. Conclusions

The CO activation over transition metal catalysts with FCC crystal phase has been systematically discussed by adopting density functional theory calculations. Based on the activation energy (E_a) of three CO activation mechanisms over different metal surfaces, we obtain that the Co and Ni metal catalysts possess better catalytic performance for CO activation. The activation energy (E_a) of three CO activation pathways over Co and Ni metal catalysts is lower than that of others. According to the density of states (DOS) and spin density plots of Co and Ni metal catalysts, we learn that Co and Ni metal catalysts show ferromagnetism, it is deduced that the catalytic activity connects the ferromagnetism. The electronic properties of metal catalysts when the small molecules (CO, CHO and COH) absorbed on the surface have been calculated, it is shown that electron transfer between the small molecules and metal catalysts happens on the unpaired *d*-orbital electrons (n_d) of metal, this electron transfer bring about the change of ferromagnetism, the more electron transfer, the greater change of ferromagnetism. The electron transfer between CHO (or COH) and metal catalysts is more than that of CO, and the carbon-oxygen bonds of CHO and COH are easier to break on the metal catalysts. So the catalytic activity connects with the metal ferromagnetism. The greater change of ferromagnetism when small molecules absorbed on the metal surface, the higher catalytic activity of metal catalyst. Meanwhile, the electron transfer bring about downshift of the *d*-band center (ε_d): the more the downshift of the *d*-band center (ε_d), the higher the catalytic activity of metal. In addition, based on the analysis of electronic properties of small molecules (the LUMO and the HOMO), it is shown that CHO and COH is more active than CO.

To summary, this DFT study about CO activation on the different metal catalysts further explains that the catalytic activity connects with the metal ferromagnetism as a result of electron transfer. It can provide a more useful and specific guide for the experiment research. The saturation magnetization (MS) of the metal catalysts can be measured by using superconducting quantum interference device (SQUID) [40], so the magnetic moments of metal catalysts can be used as an indicator to select different metal catalysts for CO activation.

CRediT authorship contribution statement

Guorong Jia: Investigation, Data curation, Writing – original draft, Formal analysis, Validation. **Lixia Ling:** Conceptualization, Investigation, Methodology, Formal analysis, Funding acquisition, Writing – review & editing. **Riguang Zhang:** Methodology, Funding acquisition. **Baojun Wang:** Resources, Funding acquisition, Supervision, Software.

Declaration of Competing Interest

The authors declare that they have no known competing financial interests or personal relationships that could have appeared to influence the work reported in this paper.

Acknowledgments

This work is financially supported by Key Projects of National Natural Science Foundation of China (No. 21736007).

Supplementary materials

Supplementary material associated with this article can be found, in the online version, at doi:10.1016/j.mcat.2021.112071.

References

[1] P. Mohanty, K.K. Pant, S.N. Naik, J. Parikh, A. Hornung, J.N. Sahu, Synthesis of green fuels from biogenic waste through thermochemical route-the role of heterogeneous catalyst: a review, Renew. Sust. Energy Rev. 38 (2014) 131–153.
[2] H.R. Yue, X.B. Ma, J.L. Gong, An alternative synthetic approach for efficient catalytic conversion of syngas to ethanol, Acc. Chem. Res. 47 (2014) 1483–1492.
[3] V. Subramani, S.K. Gangwal, A review of recent literature to search for an efficient catalytic process for the conversion of syngas to ethanol, Energy Fuels 22 (2008) 814–839.
[4] L. Shuai, L. Wang, J.H. Zhang, C. Liu, J.M. Sun, B. Peng, Y. Wang, K.G. Rappe, Y. H. Zhang, J.L. Li, L. Nie, Role of active phase in Fischer–Tropsch synthesis: experimental evidence of CO activation over single-phase cobalt catalysts, ACS Catal. 8 (2018) 7787–7798.
[5] W.Z. Li, J.X. Liu, J. Gu, W. Zhou, S.Y. Yao, R. Si, Y. Guo, H.Y. Su, C.H. Yan, W.X. Li, Y.W. Zhang, D. Ma, Chemical insights into the design and development of face-centered cubic ruthenium catalysts for Fischer–Tropsch synthesis, J. Am. Chem. Soc. 139 (2017) 2267–2276.
[6] M.M.L. Tormena, R.M. Pontes, A DFT/EDA study of ethanol decomposition over Pt, Cu and Rh metal clusters, Mol. Catal. 482 (2020) 110694–110704.
[7] S. Shetty, A.P.J. Jansen, R.A. Santen, CO dissociation on the Ru ($11\bar{2}1$) surface, J. Phys. Chem. C 112 (2008) 14027–14033.
[8] M. Ojeda, R. Nabar, A.U. Nilekar, A. Ishikawa, M. Mavrikakis, E. Iglesia, CO activation pathways and the mechanism of Fischer–Tropsch synthesis, J. Catal. 272 (2010) 287–297.
[9] C.F. Huo, J. Ren, Y.W. Li, J.G. Wang, H.J. Jiao, CO dissociation on clean and hydrogen precovered Fe (111) surfaces, J. Catal. 249 (2007) 174–184.
[10] M.O. Ozbek, J.W. Niemantsverdriet, Elementary reactions of CO and H_2 on C-terminated χ-Fe_5C_2(001) surfaces, J. Catal. 317 (2014) 158–166.
[11] T.H Pham, X.Z. Duan, G Qian, X.G. Zhou, D. Chen, CO activation pathways of Fischer–Tropsch synthesis on χ-Fe_5C_2(510): direct versus hydrogen-assisted CO dissociation, J. Phys. Chem. C 118 (2014) 10170–10176.
[12] L. Foppa, C. Coperet, A. Comas-Vives, Increased back-bonding explains step-edge reactivity and particle size effect for CO activation on Ru Nanoparticles, J. Am. Chem. Soc. 138 (2016) 16655–16668.
[13] J.E. Huheey, E.A. Keiter, R.L. Keiter, O.K. Medhi, Inorganic Chemistry: Principles of Structure and Reactivity, Pearson Education, London, 2006.
[14] Q. Zhang, L. Guo, Z.J. Hao, CO hydrogenation on M_1/W_6S_8 (M = Co and Ni) single-atom catalysts: competition between C_2 hydrocarbons and methanol synthesis pathways, Mol. Catal. 464 (2019) 10–21.
[15] J.X. Liu, H.Y. Su, D.P. Sun, B.Y. Zhang, W.X. Li, Crystallographic dependence of CO activation on cobalt catalysts: HCP versus FCC, J. Am. Chem. Soc. 135 (2013) 16284–16287.
[16] J.X. Liu, B.Y. Zhang, P.P. Chen, H.Y. Su, W.X. Li, CO dissociation on face-centered cubic and hexagonal close-packed nickel catalysts: a first-principles study, J. Phys. Chem. C 120 (2016) 24895–24903.
[17] X.B. Hao, R.G. Zhang, L.X. Ling, M.H. Fan, D.B. Li, B.J. Wang, Insight into crystal phase dependent CO dissociation on Rh catalyst from DFT and microkinetic modeling, J. Phys. Chem. C 124 (2020) 6756–6769.
[18] M.P. Andersson, F. Abild-Pedersen, I.N. Remediakis, T. Bligaard, G. Jones, J. Engbæk, O. Lytken, S. Horch, J.H. Nielsen, J. Sehested, J.R. Rostrup-Nielsen, J. K. Nørskov, I. Chorkendorff, Structure sensitivity of the methanation reaction: H_2-induced CO dissociation on nickel surfaces, J. Catal. 255 (2008) 6–19.
[19] E. Perez-Gallent, G. Marcandalli, M.C. Figueiredo, F. Calle-Vallejo, M.T.M. Koper, Structure and potential-dependent cation effects on CO reduction at copper single-crystal electrodes, J. Am. Chem. Soc. 139 (2017) 16412–16419.
[20] L. Zhong, F. Yu, Y. An, Y. Zhao, Y. Sun, Z. Li, T. Lin, Y. Lin, X. Qi, Y. Dai, L. Gu, J. Hu, S. Jin, Q. Shen, H. Wang, Cobalt carbide nanoprisms for direct production of lower olefins from syngas, Nature 538 (2016) 84–87.
[21] N. Yang, A.J. Medford, X. Liu, F. Studt, T. Bligaard, S.F. Bent, J.K. Norskov, Intrinsic selectivity and structure sensitivity of Rhodium catalysts for C_{2+} oxygenate production, J. Am. Chem. Soc 138 (2016) 3705–3714.
[22] Z.P. Liu, S.J. Jenkins, D.A. King, Step-enhanced selectivity of NO reduction on platinum-group metals, J. Am. Chem. Soc 125 (2003) 14660–14661.
[23] Y. Xu, M. Mavrikakis, Adsorption and dissociation of O_2 on gold surfaces: effect of steps and strain, J. Phys. Chem. B 107 (2003) 9298–9307.
[24] M. Behrens, F Studt, I. Kasatkin, S. Kühl, M. Havecker, F. Abild-Pedersen, S. Zander, F. Girgsdies, P. Kurr, B.L. Kniep, M. Tovar, R.W. Fischer, J.K. Nørskov, R. Schlögl, The active site of methanol synthesis Over $Cu/ZnO/Al_2O_3$ industrial catalysts, Science 336 (2012) 893–897.

[25] A. Cao, J.L. Schumann, T. Wang, L.N. Zhang, J.P. Xiao, P. Bothra, Y. Liu, F. Abild-Pedersen, J.K. Norskov, Mechanistic insights into the synthesis of higher alcohols from syngas on CuCo alloys, ACS Catal. 8 (2018) 10148–10155.

[26] K.W. Yang, M.H. Zhang, Y.Z. Yu, Effect of transition metal-doped Ni(211) for CO dissociation: insights from DFT calculations, Appl. Surf. Sci. 399 (2017) 255–264.

[27] F.R. García-García, A. Guerrero-Ruiz, I. Rodríguez-Ramos, Role of B5 type sites in Ru catalysts used for the NH_3 decomposition reaction, Top. Catal. 33 (2009) 758–764, 52.

[28] P.V. Helden, I.M. Ciobîca, R.L.J. Coetzer, The size-dependent site composition of FCC cobalt nanocrystals, Catal. Today 261 (2016) 48–59.

[29] D.A.J.M. Ligthart, I.A.W. Filot, A.A.H. Almutairi, E.J.M. Hensen, Identification of step-edge sites on Rh nanoparticles for facile CO dissociation, Catal. Commun. 77 (2016) 5–8.

[30] K. Honkala, A. Hellman, I.N. Remediakis, Ammonia synthesis from first-principles calculations, Science 307 (2005) 555–558.

[31] M.A. Vannice, The catalytic synthesis of hydrocarbons from H_2CO mixtures over the group VIII metals: I. The specific activities and product distributions of supported metals, J. Catal. 37 (1975) 449–461.

[32] M. Gupta, M.L. Smith, J.J. Spivey, Heterogeneous catalytic conversion of dry syngas to ethanol and higher alcohols on Cu-based catalysts, ACS Catal. 1 (2011) 641–656.

[33] M. Ao, G.H. Pham, J. Sunarso, M.O. Tade, S.M. Liu, Active centers of catalysts for higher alcohol synthesis from syngas: a Review, ACS Catal. 8 (2018) 7025–7050.

[34] D. Wang, L. Chen, G.C. Li, Z. Wang, X.B. Li, B. Hou, Cobalt-based Fischer-Tropsch synthesis: effect of the catalyst granule thermal conductivity on the catalytic performance, Mol. Catal. 502 (2021) 111395–111401.

[35] G. Brodén, T.N. Rhodin, C. Brucker, Synchrotron radiation study of chemisorptive bonding of CO on transition metals-Polarization effect on Ir(100), Surf. Sci. 59 (1976) 593–611.

[36] K. Cheng, J.C. Kang, D.L. King, V. Subramanian, C. Zhou, Q.H. Zhang, Y. Wang, Advances in catalysis for syngas conversion to hydrocarbons, Adv. Catal. 60 (2017) 125–208.

[37] J.K. Sun, H.X. Zhao, X. Fang, S.L. Zhai, D. Zhai, L. Sun, Theoretical studies on the catalytic hydrogenation of carbon dioxide by 3d transition metals single-atom catalyst supported on covalent triazine frameworks, Mol. Catal. 508 (2021) 111581–111589.

[38] G.J. Chen, S.Y. Wu, First-principles study of AuS_n ($2 \leq n \leq 7$) clusters: structural, electronic, magnetic, spectral properties, and adsorption properties with O_2 and H_2O, J. Nanopart. Res. 22 (2020) 1–19.

[39] B.D. Cullity, C.D. Graham, Introduction to Magnetic Materials, 2nd ed., IEEE Press, 2009.

[40] Y.B. Zhai, J. Zhang, J.Q. Sun, Y.Y. Xue, Z. Chen, M. Chen, B.H. Wang, J.G. Chen, The effect of the unpaired d-orbital electron number in Fe and Co catalysts on Fischer–Tropsch synthesis, Catal. Sci. Technol. 6 (2016) 7942–7945.

[41] D.O. Hayward, Chemisorption and Reactions on Metallic Films, 34, Academic Press, 1971, pp. 225–326.

[42] O.O. James, B. Chowdhury, M.A. Mesubi, S. Maity, Reflections on the chemistry of the Fischer–Tropsch synthesis, RSC Adv. 2 (2012) 7347–7366.

[43] J.L. Wang, Y.B. Wang, G.F. Wu, X.Y. Zhang, X.J. Zhao, M.L. Yang, *Ab* initio study of the structure and magnetism of atomic oxygen adsorbed Sc_n ($n = 2$–14) clusters, Phys. Chem. Chem. Phys. 11 (2009) 5980–5985.

[44] Y.N. Tang, Z.X. Yang, X.Q. Dai, D.W. Ma, Z.M. Fu, Formation, stabilities, and electronic and catalytic performance of platinum catalyst supported on non-metal-doped graphene, J. Phys. Chem. C 117 (2013) 5258–5268.

[45] J.L. Du, G.F. Wu, J.L. Wang, Density functional theory study of the interaction of carbon monoxide with bimetallic Co-Mn clusters, J. Phys. Chem. A 114 (2010) 10508–10514.

[46] G. Kresse, J. Furthmüller, Efficient iterative schemes for *ab* initio total-energy calculations using a plane-wave basis set, Phys. Rev. B 54 (1996) 11169–11186.

[47] G. Kresse, J. Furthmüller, Efficiency of *ab*-initio total energy calculations for metals and semiconductors using a plane-wave basis set, Comput. Mater. Sci. 6 (1996) 15–50.

[48] J.P. Perdew, K. Burke, M. Ernzerhof, Generalized gradient approximation made simple, Phys. Rev. Lett. 77 (1996) 3865–3868.

[49] J.A. White, D.M. Bird, Implementation of gradient-corrected exchange-correlation potentials in car-parrinello total-energy calculations, Phys. Rev. B 50 (1994) 4954–4957.

[50] H.J. Monkhorst, J.D. Pack, Special points for Brillonin-zone integrations, Phys. Rev. B 13 (1976) 5188–5192.

[51] D. Sheppard, P. Xiao, W. Chemelewski, D.D. Johnson, G. Henkelman, A generalized solid-state nudged elastic band method, J. Chem. Phys. 136 (2012), 074103–1-8.

[52] D. Sheppard, T. Rye, G. Henkelman, Optimization methods for finding minimum energy paths, J. Chem. Phys. 128 (2008) 1–10.

[53] M.R. Elahifard, M.P. Jigato, J.W. Niemantsverdriet, Direct versus hydrogen-assisted CO dissociation on the Fe(100) surface: a DFT study, ChemPhysChem 13 (2012) 89–91.

[54] M.P. Andersson, E. Abild-Pedersen, I.N. Remediakis, T. Bligaard, G. Jones, J. Engbwk, O. Lytken, S. Horch, J.H. Nielsen, J. Seheste, Structure sensitivity of the methanation reaction: H_2-induced CO dissociation on nickel surfaces, J. Catal. 255 (2008) 6–19.

[55] W. Wang, Y. Wang, G.C. Wang, CO Dissociation mechanism on Pd-doped Fe(100): a comparison with Cu/Fe(100), J. Phys. Chem. C 121 (2017) 6820–6834.

[56] F. Studt, F. Abild-Pedersen, Q.X. Wu, A.D. Jensen, B. Temel, J.D. Grunwaldt, J. K. Norskov, CO hydrogenation to methanol on Cu–Ni catalysts: theory and experiment, J. Catal. 293 (2012) 51–60.

[57] S. Dahl, A. Logadottir, C.J.H. Jacobsen, J.K. Nørskov, Electronic factors incatalysis: the volcano curve and the effect of promotion in catalytic ammonia synthesis, Appl. Catal. A Gen. 222 (2001) 19–29.

[58] T. Bligaard, J.K. Nørskov, S. Dahl, J. Matthiesen, C.H. Christensen, J. Sehested, The Brønsted–Evans–Polanyi relation and the volcano curve in heterogeneous catalysis, J. Catal. 224 (2004) 206–217.

[59] X.B. Li, S.R. Wang, Y.Y. Zhu, G. Chen, G.H. Yang, Density functional theory study of ethanol synthesis from dimethylether and syngas over cobalt catalyst, Mol. Catal. 432 (2017) 115–124.

[60] Y.M. Choi, P. Liu, Mechanism of ethanol synthesis from syngas on Rh(111), J. Am. Chem. Soc. 131 (2009) 13054–13061.

[61] N.Y. Yang, A.J. Medford, X.Y. Liu, F. Studt, T. Bligaard, S.F. Bent, J.K. Nørskov, Intrinsic selectivity and structure sensitivity of Rhodium catalysts for C_{2+} oxygenate production, J. Am. Chem. Soc. 138 (2016) 3705–3714.

[62] P.M. Patterson, T.K. Das, B.H. Davis, Carbon monoxide hydrogenation over molybdenum and tungsten carbides, Appl. Catal. A Gen. 251 (2003) 449–455.

[63] D.V.N. Vo, T.H. Nguyen, E.M. Kennedy, B.Z. Dlugogorski, A.A. Adesina, Fischer–Tropsch synthesis: effect of promoter type on alumina-supported Mo carbide catalysts, Catal. Today 175 (2011) 450–459.

[64] Y. Zhao, B. Zhao, J. Liu, G. Chen, R. Gao, S. Yao, M. Li, Q. Zhang, L. Gu, J. Xie, X. Wen, L. Wu, C. Tung, D. Ma, T. Zhang, Oxide-modified nickel photocatalysts for the production of hydrocarbons in visible light, Angew. Chem. Int. Ed. 55 (2016) 4215–4219.

[65] H.Y. Gong, Y.R. He, J.Q. Yin, S.Y. Liu, M.Q. Peng, C.F. Huo, H. Wang, Y. Yang, X. D. Wen, Electronic effects of transition metal dopant Fe(100) and Fe_5C_2(100) surfaces for CO activation, Catal. Sci. Technol. 10 (2020) 2047–2056.

[66] A.J. Medford, A.C. Lausche, F. Abild-Pedersen, B. Temel, N.C. Schjødt, J. K. Nørskov, F. Studt, Activity and selectivity trends in synthesis gas conversion to higher alcohols, Top. Catal. 57 (2014) 135–142.

[67] S. Kattel, P. Atanassov, B. Kiefer, Electronic and magnetic properties of in-plane defects in graphene: a first-principles study, J. Phys. Chem. C 116 (2012) 8161–8166.

[68] M. Battocletti, H. Ebert, H. Akai, Influence of gradient corrections to the local-density-approximation on the calculation of hyperfine fields in ferromagnetic Fe, Co, and Ni, Phy. Rev. B 53 (1996) 9776–9783.

[69] J.D. Li, E. Croiset, L. Ricardez-Sandoval, Methane dissociation sociation on Ni (100), Ni(111), and Ni(553): a comparative density functional theory study, J. Mol. Catal. A Chem. 365 (2012) 103–114.

[70] F. Besenbacher, I. Chorkendorff, B.S. Clausen, B. Hammer, A.M. Molenbroek, J. K. Nørskov, I. Stensgaard, Design of a surface alloy catalyst for steam reforming, Science 279 (1998) 1913–1915.

[71] A. Ruban, B. Hammer, P. Stoltze, H.L. Skriver, J.K. Nørskov, Surface electronic structure and reactivity of transition and noble metals, J. Mol. Catal. A Chem. 115 (1997) 421–429.

[72] K.F. Khaled, Adsorption and inhibitive properties of a new synthesized guanidine derivative on corrosion of copper in 0.5M H_2SO_4, Appl. Surf. Sci. 255 (2008) 1811–1818.

[73] Y.H. Zhao, K.J. Sun, X.F. Ma, J.X. Liu, D.P. Sun, H.Y. Su, W.X. Li, Carbon chain growth by formyl insertion on rhodium and cobalt catalysts in syngas conversion, Angew. Chem. 123 (2011) 5447–5450.